








RESEARCH ARTICLE | FEBRUARY 27 2024

# Numerical simulation of droplet impacting on a microstructured surface: Geometry, wettability, and control of jump-off force

Xi Gu ; Li Chen ; Feng Wang; Yingrui Wang ; Yuqi Li; Wenna Wu; Man Hu  ; Daosheng Deng  

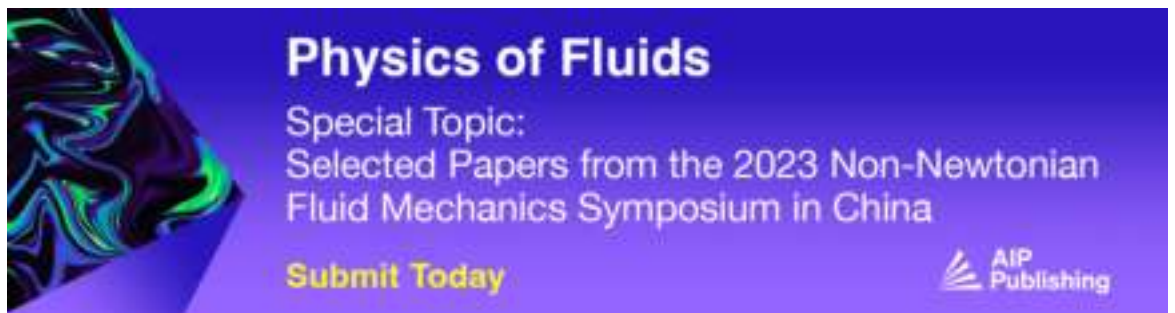


*Physics of Fluids* 36, 022025 (2024)


<https://doi.org/10.1063/5.0190154>



CrossMark



**Physics of Fluids**  
Special Topic:  
Selected Papers from the 2023 Non-Newtonian  
Fluid Mechanics Symposium in China  
**Submit Today**



# Numerical simulation of droplet impacting on a microstructured surface: Geometry, wettability, and control of jump-off force

Cite as: Phys. Fluids **36**, 022025 (2024); doi: 10.1063/5.0190154

Submitted: 4 December 2023 · Accepted: 24 January 2024 ·

Published Online: 27 February 2024



Xi Gu, Li Chen, Feng Wang, Yingrui Wang, Yuqi Li, Wenna Wu, Man Hu,<sup>a)</sup> and Daosheng Deng<sup>a)</sup>

## AFFILIATIONS

Department of Aeronautics and Astronautics, Fudan University, Shanghai 200433, China

<sup>a)</sup>Authors to whom correspondence should be addressed: [human@fudan.edu.cn](mailto:human@fudan.edu.cn) and [dsdeng@fudan.edu.cn](mailto:dsdeng@fudan.edu.cn)

## ABSTRACT

Droplet impacting on the solid substrate, which typically is a simple planar surface, has been extensively studied for various technological applications. Here, through numerical calculation, we explore the droplet impacting on a single hemispherical bead and double bead structures. Several key physical parameters have been taken into account, including the Weber number, wettability, and geometry of microstructures. We reveal the spatiotemporal evolution of the droplet pattern, the correlated physical parameters, and the underlying physical mechanisms (air cushion or bubble). These results provide theoretical guidance to control jump-off forces via the structure design and suitable wettability for the relevant applications such as erosion protection.

Published under an exclusive license by AIP Publishing. <https://doi.org/10.1063/5.0190154>

## I. INTRODUCTION

Droplet impacting on solid surfaces not only exhibits the intriguing dynamical patterns, but also holds substantial technological applications.<sup>1,2</sup> For example, the interaction between droplets and non-planar superhydrophobic surfaces is indispensable to self-cleaning<sup>3</sup> and anti-icing<sup>4</sup> for wires, cables, or antennas. Schutzius *et al.*<sup>5</sup> proposed the use of wettability-engineered surfaces to manipulate the impacting droplets for microfluidics and fluid-assisted templating applications.

The dynamics of droplet impacting on solid surfaces is extremely complicated, as determined collectively by several physical parameters, including impact velocity, relative impact direction, droplet size, and liquid properties.<sup>6–9</sup> Generally, dimensionless Weber number and wettability offer a comparative basis across various experimental and theoretical studies.<sup>10–13</sup> The Weber number is defined as  $We = \rho V_i^2 d / \sigma$ , where  $\rho$ ,  $\sigma$ ,  $d$ , and  $V_i$  represent the liquid's density, surface tension, droplet diameter, and impact velocity, respectively. Also, surface wettability can significantly influence droplet impacting dynamics<sup>2,14–21</sup> and is characterized by the contact angle (C.A.).<sup>22</sup> For example, superhydrophobic surfaces refer to high contact angles (often exceeding 150°) and very low contact angle hysteresis (generally less than 10°).<sup>23</sup> In contrast, hydrophilic surfaces exhibit small contact angles, typically below 90°, promoting efficient droplet spreading.<sup>24</sup> The intermediate range between these two extremes is designated as hydrophobic surfaces. Interestingly, when droplet falling on superhydrophobic surfaces,

a distinct peak of the normal force during the rebound stage has been recently identified, emerging through flow focusing to generate a Worthington jet.<sup>20,21,25,26</sup>

Droplet impacting on non-planar surfaces, such as cylindrical wires and solid spheres, has been explored primarily through experimental approaches, yielding insights into post-impingement behaviors and the formation of impinging droplet crowns.<sup>27–30</sup> Yada *et al.*<sup>31</sup> used a high-speed camera to study droplet impact on surfaces with inclined micropillars. Qian *et al.*<sup>32</sup> studied the dynamic behavior of droplets impacting cylindrical superhydrophobic surfaces with different structures, such as azimuthal grooves, axial grooves, and pillars. Li *et al.*<sup>26</sup> designed a superhydrophobic substrate with a specific ridge to break the symmetry of flow focusing and weaken the droplet jump-off force, shedding light on the erosion protection.

On the other hand, numerical simulations can provide a more insightful understanding of droplet impacting dynamics on curved surfaces and other microstructures.<sup>33–37</sup> Liu *et al.*<sup>38</sup> conducted numerical research on the dynamic characteristics of a droplet impacting a hydrophobic tube. Liu *et al.*<sup>39</sup> studied the sharp interface cartesian grid method, a technique for simulating droplet interactions with surfaces of arbitrary shape. This fixed-grid, sharp interface method is designed to simulate droplet impact and spreading on complicated surfaces. Khojasteh *et al.* conducted three-dimensional numerical simulations through level-set method to investigate water droplet impact on both

curved and flat hydrophobic and superhydrophobic substrates.<sup>18</sup> Abubakar *et al.*<sup>40</sup> explored the impact of droplets on a hydrophobic surface, focusing on the influence of surface wetting state on droplet behavior. These simulations aim to explore both bouncing and non-bouncing cases, expanding from two-dimensional models to three-dimensional representations.

The volume of fraction (VoF) method is another numerical tool employed to track the gas–liquid interface. Pasandideh-Fard *et al.*<sup>41</sup> investigated capillary effects during droplet impact on a solid surface, using a numerical solution of the Navier–Stokes equation with a modified Solution algorithm volume of fraction (SOLA-VoF) method to model droplet deformation. Comparison of computer generated images of impacting droplets with photographs confirmed the accuracy of the numerical model in predicting droplet shape evolution. Blake *et al.*<sup>42</sup> performed simulations in ANSYS Fluent using a coupled VoF and level-set method to capture the air–water interface, and an enthalpy-porosity method is used to capture the liquid–solid interface. The simulation strategy successfully predicts the overall droplet response for several droplet impact conditions.

In this work, the primary objective is to conduct a comprehensive investigation into the dynamics of droplet impacting on complicated microstructures through numerical simulation. A two-dimensional model is developed to analyze the influence of various parameters, including Weber numbers, wettability, bead size, and spacing between beads on substrates, and parallel computation techniques are utilized to enhance computational efficiency. The volume of fraction (VoF) method is employed to track the liquid–gas interface in the multiphase flow, and the reliability and accuracy of the numerical method are verified through comparisons with experimental data and theoretical solutions. We will reveal the spatiotemporal evolution of the droplet pattern, the correlated physical parameters and the underlying physical mechanisms (air cushion or bubble), allowing the controllable jump-off force via the structure design and suitable wettability.

## II. GOVERNING EQUATIONS

In the numerical simulation, the governing equations for the entire liquid–gas (water–air) domain are the momentum and continuity equations<sup>43</sup> as follows:

$$\frac{\partial(\rho\mathbf{u})}{\partial t} + \nabla \cdot (\rho\mathbf{u}\mathbf{u}) = -\nabla p + \nabla \cdot \boldsymbol{\tau} + \rho\mathbf{g} + \mathbf{F}, \quad (1a)$$

$$\nabla \cdot \mathbf{u} = 0, \quad (1b)$$

$$\frac{\partial\alpha}{\partial t} + \mathbf{u} \cdot \nabla\alpha = 0. \quad (1c)$$

Here, Eq. (1a) is the Navier–Stokes equation for the momentum, where  $\rho$ ,  $p$ ,  $\mathbf{g}$ , and  $\mathbf{F}$  represent density, pressure, gravity, and surface tension force, respectively. In the current study, the gravity is  $9.8 \text{ m/s}^2$ . Equation (1b) is the continuity equation for the incompressible water. Term  $\nabla \cdot \boldsymbol{\tau}$  in Eq. (1a) is calculated by

$$\nabla \cdot \boldsymbol{\tau} = \nabla \cdot (\nu\nabla\mathbf{u}) + \nabla\mathbf{u} \cdot \nabla\nu. \quad (2)$$

The surface tension force  $\mathbf{F}$  is defined as

$$\mathbf{F} = \sigma \left[ \nabla \cdot \left( \frac{\nabla\alpha}{|\nabla\alpha|} \right) \right] (\nabla\alpha), \quad (3)$$

where  $\mathbf{n} = \frac{\nabla\alpha}{|\nabla\alpha|}$  is the unit vector normal to the interface and  $\sigma$  is the interfacial tension at the liquid–gas (water–air) interface.

Here, the phase function  $\alpha$  is calculated by Eq. (1c), where  $\alpha = 1$  for water,  $\alpha = 0$  for air, and  $\alpha = 0.5$  represents the air–water interface. Density  $\rho$  and viscosity  $\nu$  can be expressed as

$$\rho = \alpha\rho_1 + (1 - \alpha)\rho_2, \quad (4)$$

$$\nu = \alpha\nu_1 + (1 - \alpha)\nu_2, \quad (5)$$

where  $\rho_1$  and  $\nu_1$  are the density and viscosity of water and  $\rho_2$  and  $\nu_2$  are the density and viscosity of air.

## III. NUMERICAL MODEL AND VALIDATION

Figure 1(a) illustrates a two-dimensional droplet impact model, which is designed to facilitate parallel computation with OpenFOAM. The top and side boundaries are exposed to the atmosphere, while the bottom boundary is set as the impacted substrate with varying contact angles ( $C.A.$ ) to analyze the effect of wettability. A structured mesh is generated by blockMesh, and the grid size is standardized to encompass regions where the droplet may spread, rebound, or splash under any circumstances. The droplet’s radius is denoted as  $r$ , and the initial center position is  $(0, r)$ . The computational domain measures  $12 \times 24 \text{ mm}^2$ , consisting of  $1200 \times 2400$  cells. It is decomposed into 64 parts of  $8 \times 8$ , each for parallel computation using 64 processors. The multiphaseinterFoam solver is employed to implement the volume of fraction (VoF) method.

The procedure of parallel computation is demonstrated in Fig. 1(b). We first initialize the mesh, boundary conditions, internal fields, and the initial conditions of the droplet, including its position and velocity, as illustrated in Fig. 1(a). Next, the computational domain is decomposed into  $8 \times 8$  sections, to enable parallel computation, which allows for efficient processing of the simulation. Subsequently, the time step size for each iteration is updated, following the calculation of interested variables, such as the volume fraction of air and water, along with other relevant quantities. The process of updating the time step and computing the variables are repeated if the simulation continues. Finally, the outputs from all processors involved in the simulation are reconstructed for further analysis and interpretation of the results.

Four grid sizes, 5, 10, 20, and  $40 \mu\text{m}$ , is tested in Fig. 1(c), and the grid size of  $10 \mu\text{m}$  is adopted to ensure both accuracy and calculation efficiency. Figure 1(d) presents a quantitative validation with experimental measurements and Wagner theory.<sup>44</sup> Droplets with  $We$  of 34 and 134 are scrutinized for validation purposes. The  $y$ -axis,  $L$ , denotes the radial length of the turning point. As inferred from the comparison, the computed results align well with the experimental data, as shown by the typical snapshots in Fig. 1(e). The minor discrepancy between the numerical prediction and theoretical solution likely arises from the fact that Wagner theory does not account for the viscosity of fluids, as denoted by  $L = \sqrt{3rV_b t}$ , where  $r$ ,  $V_b$ , and  $t$  are the initial radius, initial velocity of an impacting droplet, and the time after impacting.

## IV. RESULTS AND DISCUSSIONS

### A. Impacting forces on microstructures

Figure 2 depicts the model sketch and impacting force of a water droplet (radius,  $r = 0.6 \text{ mm}$ ) on various microstructures. Here, we

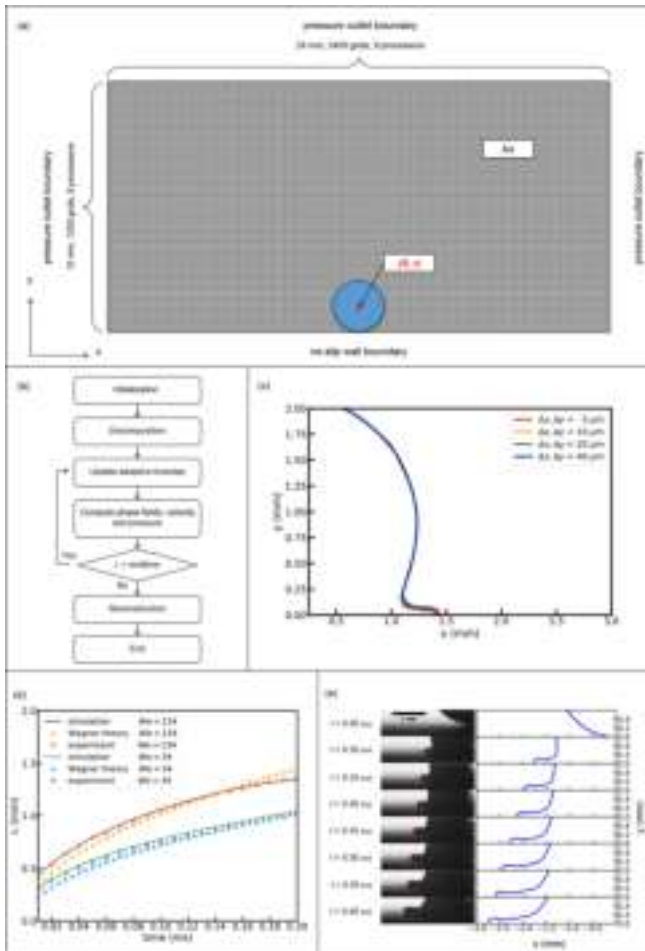


**FIG. 1.** A two-dimensional droplet impacting model is adopted in this study to allow parallel calculation with OpenFOAM.<sup>43</sup> In (a), the domain is filled with structured mesh and the grid size is uniformed to encase the regions where the drop will spread or rebound in either case. The radius of drop is  $r$ , and the initial center position is  $(0, r)$ . The computational domain is  $12 \times 24 \text{ mm}^2$ , with  $1200 \times 2400$  cells, decomposed into  $8 \times 8$  parts for parallel computation using 64 processors. (b) A flow chart of parallel computation. (c) Predicted shape outlines of four grid sizes, 5, 10, 20, and  $40 \mu\text{m}$  are tested to verify the numerical model. (d) Numerical simulation of droplet impacting on hydrophilic substrates (at Weber number  $We = 34$  and 134) validated with experimental measurements and Wagner theory, and the y-axis indicates the radial length of the turning point. (e) The snapshot comparison between the experimental observation [indicated by the green dots in (d), the red line indicating for the substrate] and the numerical prediction [indicated by the dash line in (d)] of a water drop impacting on the hydrophilic substrates.

mainly investigate the following three cases of the geometry: (a) a flat substrate, (b) a single bead, and (c) double beads.

The instantaneous impacting force  $F$  is calculated by the following equation:

$$F = \sum_{i=1}^n \Delta P_i \cdot \Delta x_i \cdot \delta, \quad (6)$$

where  $n = 1, 200$  is the number of grids along the x-axis of the model,  $\Delta P_i$  is the localized pressure change,  $\Delta x_i$  is the length of a grid, and

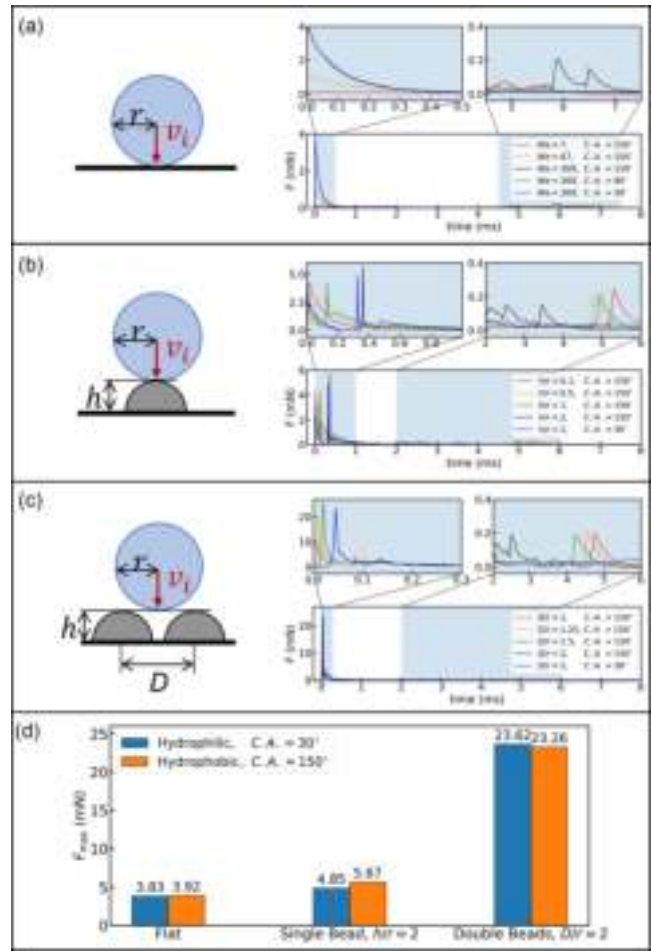


**FIG. 2.** Time-dependent droplet impacting forces on various microstructures: (a) a flat substrate, (b) a single hemispherical bead, and (c) double hemispherical beads. (d) Maximum impacting force dependent on wettability and microstructures. [ $r = 0.6 \text{ mm}$ ;  $We = 269$  and  $C.A. = 150^\circ$  for (b) and (c); and  $h/r = 0.5$  in (c);  $We = 269$  in (d)]. Multimedia available online.

$\delta = 0.1 \text{ mm}$  is the virtual thickness of the two-dimensional computational domain.

For the case of a flat substrate, the effect of  $We$  and  $C.A.$  is examined shown in Fig. 2(a) (Multimedia view). Initially, the impacting force increases with time and reaches a peak value or primary peak force, as the droplet touching down the substrate and spreading along the substrate. At this stage, the pronounced primary force is enhanced with  $We$  as shown by the enlarged inset from 0 to 0.5 ms, and clearly, the elevated force corresponds to  $We = 269$  (the blue line). Afterward, the force gradually decreases, but there might be a secondary peak force associated with the hydrophobic surface at high  $We$ , such as  $C.A. = 150^\circ$  and  $We = 269$  (the black line), as indicated by the enlarged inset from 5 to 7 ms. This secondary peak force is consistent with the recent study of jump-off peak force for a water droplet falling on superhydrophobic surfaces.<sup>20,21,25</sup>

For the case of a single bead (similar to a ridged surface<sup>26</sup>), the impacting forces become much more complicated than that of the flat

surface, and Fig. 2(b) (Multimedia view) demonstrates the effect of bead size by controlling the ratio of  $h/r = 0.1, 0.5, 1,$  and  $2$ . The second peak force, higher than the initial impacting force, is captured from  $0.1$  to  $0.4$  ms for  $h/r = 1$  and  $2$  (indicated by the green, black, and blue lines). Additionally, lower force peaks are observed when droplet fragments rebound at around  $5$  ms for  $h/r = 0.1, 0.5,$  and  $1$  (indicated by the red, yellow, and blue lines).

For the case of double beads, the primarily peak force becomes much higher as indicated in Fig. 2(c) (Multimedia view) for the same  $We = 269$  as in Fig. 2(b). The initial impacting forces peak reaches over  $20$  mN, when  $D/r > 1$  (indicated by the yellow, green, black, and blue lines).

For various cases, the maximum impacting forces ( $F_{max}$ ) at a given  $We$  are presented in Fig. 2(d). For hydrophilic surface  $C.A. = 30^\circ$  and hydrophobic surface  $150^\circ$ , the similar  $F_{max}$  indicates the primary peak force might be independent of the wettability. For a double-bead structure, the significant increased  $F_{max}$  likely arises from the entrapped or compressed air between the two beads, resulting in the elevated high pressure. Since the gas is assumed to be incompressible in the simulation, this enhanced  $F_{max}$  might be overestimated compared to the compressible air, and would require future experimental verification.

### B. Splashing satellite droplets at the peak force

Figure 3 shows the pressure change  $\Delta P = P - P_0$  and normalized velocity magnitude  $\tilde{V} = V/V_i$  when a water drop of radius  $r = 0.6$  mm impacts on (a) a flat substrate, (b) a single bead, and (c) double beads at a high  $We = 269$  upon non-wettable hydrophobic surface  $C.A. = 150^\circ$ . Figure 3(a) presents that the jump-off force or local peak force is caused by a splashing droplet rebounding vertically on a flat substrate at (ii) time  $t = 6.00$  ms and (iii)  $6.50$  ms. Also, Fig. 3(b) illustrates that the satellite droplets splash side-way when it impacts a single bead or double beads. However, as shown in Fig. 3(c), nearly a half of the droplet is trapped between the beads at (iii) and (iv), so there is no jump-off peak force observed under this situation. It should be noticed that the entire droplet bounces off from the substrate in only  $4$  ms in Fig. 3(b). Therefore, the non-wettable hydrophobic surface with an array of single beads might be a potential solution for erosion protection due to the short contact time of the impacting droplet.

### C. Case of a flat surface: Wettability

Figure 4 demonstrates the pressure and phase field evolution at a given high  $We = 269$ , dependent on the wettability for (a)  $C.A. = 150^\circ$ , (b)  $C.A. = 90^\circ$ , and (c)  $C.A. = 30^\circ$ . Here,  $\Delta P = P - P_0$  is defined as the pressure change along x-axis over time. Upon impacting on hydrophobic surfaces with various  $We$ , droplets undergo two distinct phases: (i) spreading and (ii) retracting, as illustrated in Figs. 2(a) and 4. (i) During the initial spreading stage, the droplet becomes flattened, because the kinetic energy is converted into interfacial energy, accompanied by minimal energy dissipation. (ii) Subsequently, the droplet is retracted to recover a spherical shape before eventually detaching in the vertical direction. It is noteworthy that prior research has unveiled phenomena associated with droplet impacting on hydrophobic surfaces, including rebounding, where the droplet bounces off the surface, typically observed at a lower  $We$  or impact velocities. However, at a higher  $We$  exceeding a critical threshold, the droplet shatters into several

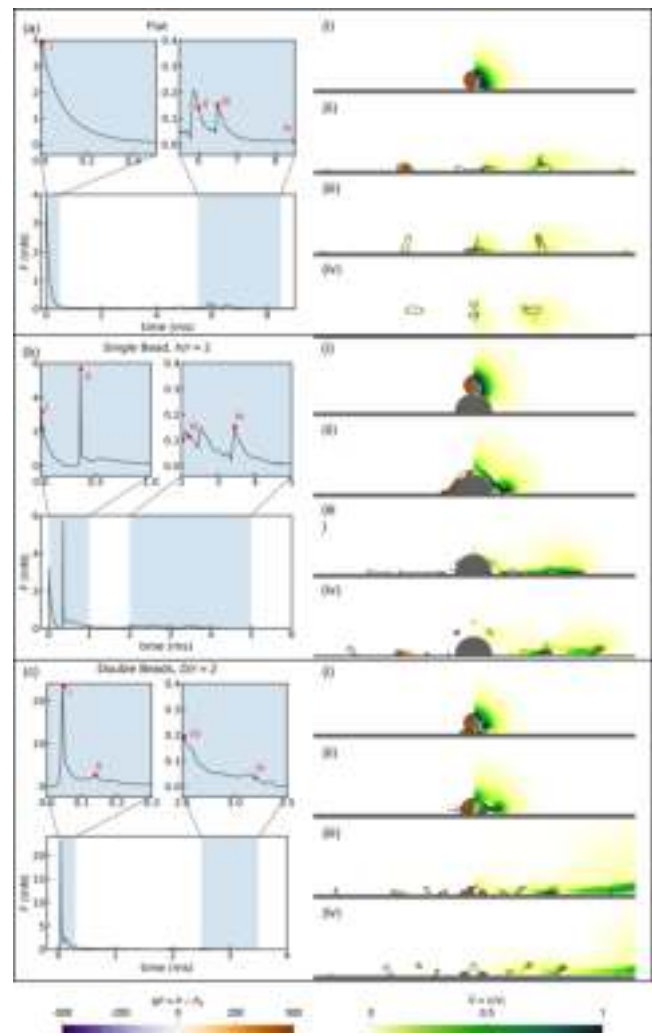


FIG. 3. For the splashing satellite droplets peak force, the associated pressure change ( $\Delta P = P - P_0$ , the right panel of the snapshot) and normalized velocity magnitude ( $\tilde{V} = V/V_i$ , the left panel of the snapshot), when a water drop of radius  $r = 0.6$  mm impacts on (a) a flat substrate, (b) a single bead ( $h/r = 2$ ), and (c) double beads ( $D/r = 2$ ) ( $We = 269$  and  $C.A. = 150^\circ$ ).

fragments before bouncing off the substrate, leading to a splashing phenomenon as depicted in Fig. 4(a). It should be noted that in Fig. 4(b), a minor portion of the droplet remains on the substrate while the majority detaches after impacting a hydrophilic surface of  $C.A. = 90^\circ$ . Additionally, the droplet in Fig. 4(c) does not bounce off after retracting if  $C.A.$  is as low as  $30^\circ$ .

Despite the distinctive impacting dynamics and the morphology evolution, the color-maps of pressure have the similar trend, and the initial pronounced pressure at the center gradually spreads outward to form a red cone shape in the map.

### D. Case of a single bead: Bead size

Figure 5 presents the pressure variation,  $\Delta P = P - P_0$ , along the x axis and the trapped air cushions and air bubbles for the different

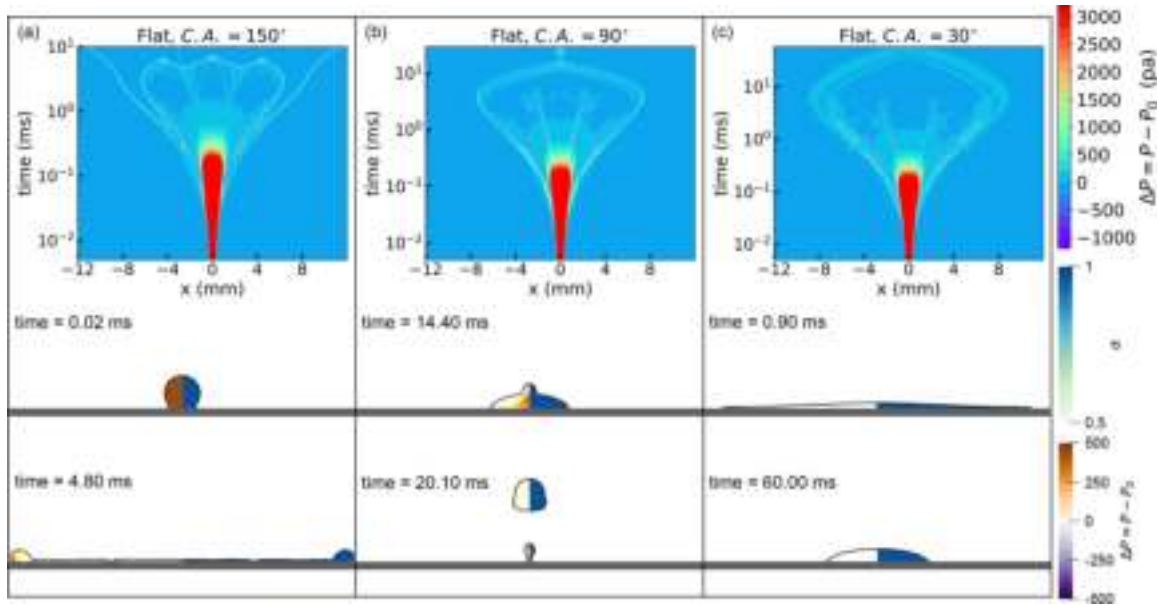


**FIG. 4.** For the case of flat substrate, the effect of wettability on pressure changeover time ( $\Delta P = P - P_0$ , along the  $x$  axis): (a)  $C.A. = 150^\circ$ , (b)  $C.A. = 90^\circ$ , and (c)  $C.A. = 30^\circ$ . The left and right panel of the snapshot for the pressure and the volume fraction of water ( $\alpha$ ). The schematic view of the models is illustrated in Fig. 2(a),  $We = 269$ .

situations, (a)  $h/r = 0.1, C.A. = 150^\circ$ , (b)  $h/r = 2, C.A. = 150^\circ$ , and (c)  $h/r = 2, C.A. = 30^\circ$ . As shown in Fig. 5(a), the small and tiny bead punctures a hole at the center of the spreading droplet, causing the water to retract in the opposite direction where it breaks. Similar phenomena are observed for  $h/r = 0.5$  and 1.

However, when the size of the bead surpasses that of the droplet ( $h/r = 2$ ) as shown in Fig. 5(b), the impacting droplet quickly disintegrates into multiple fragments and splashes, causing a fluctuation of force [represented by the black line in Fig. 2(b)]. Noticeably, air cushions and bubbles are captured in Figs. 5(b) and 5(c). A larger amount

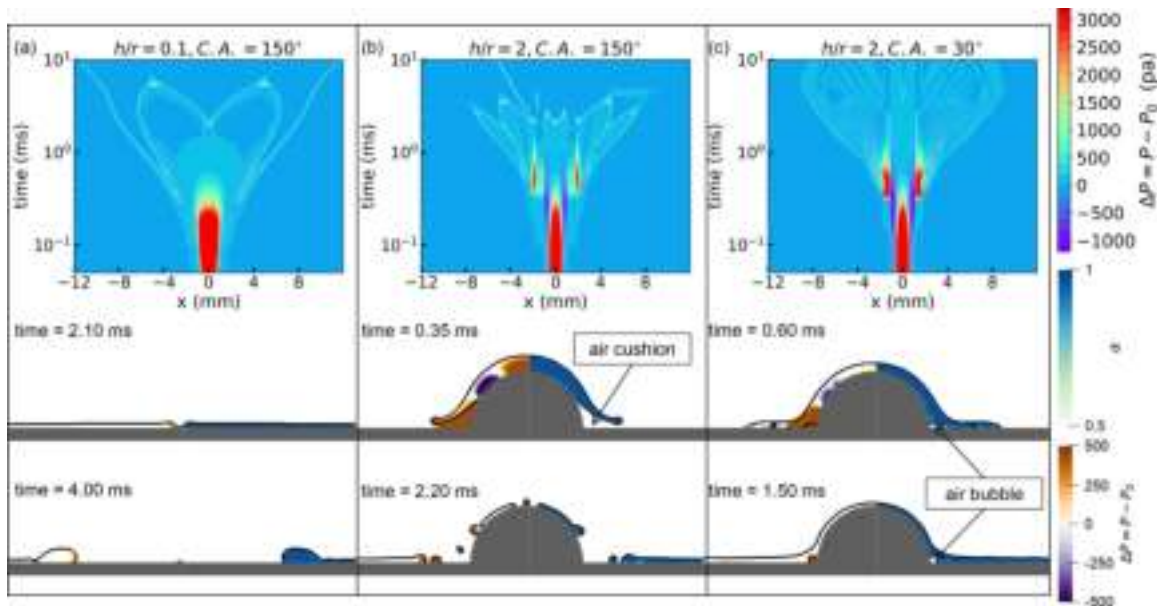


**FIG. 5.** For the case of a single bead, effect of  $h/r$  and  $C.A.$  on pressure variation,  $\Delta P = P - P_0$ , along the  $x$  axis and inside air cushions, (a)  $h/r = 0.1, C.A. = 150^\circ$ , (b)  $h/r = 2, C.A. = 150^\circ$ , and (c)  $h/r = 2, C.A. = 30^\circ$ . The left and right panel of the snapshot for the pressure and the volume fraction of water ( $\alpha$ ). The schematic view of the models is illustrated in Fig. 2(b),  $We = 269$ .

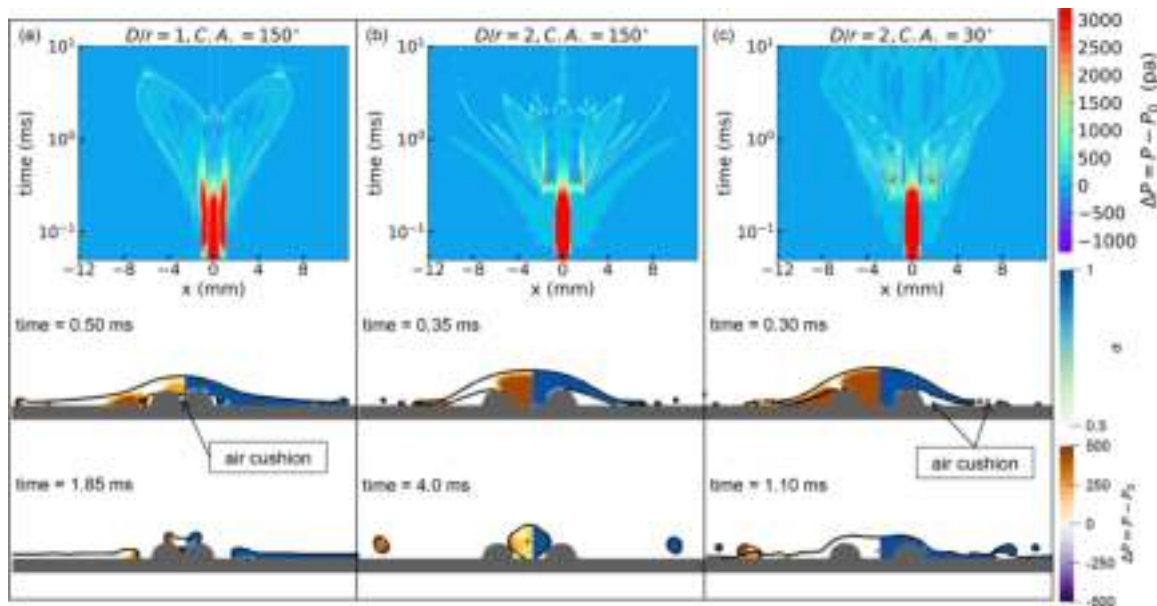


**FIG. 6.** For the case of double beads, the effect of  $D/r$  and  $C.A.$  on pressure variation,  $\Delta P = P - P_0$ , along the  $x$  axis and inside air cushions, (a)  $D/r = 1$ ,  $C.A. = 150^\circ$ , (b)  $D/r = 2$ ,  $C.A. = 150^\circ$ , and (c)  $D/r = 2$ ,  $C.A. = 30^\circ$ . The left and right panel of the snapshot for the pressure and the volume fraction of water ( $\alpha$ ). The schematic view of the models are illustrated in Fig. 2(c),  $h/r = 0.5$  and  $We = 269$ .

of air is trapped when droplet impacting the bead on a hydrophobic substrate than on a hydrophilic surface. The expanding thin water layer over the large air cushion in Fig. 5(b) leads to a quick collapse and splash, whereas small air bubbles are trapped at the edge of the bead during the expansion stage in Fig. 5(c). Neither bouncing nor jump-off force is observed when impacting a hydrophilic surface.

### E. Case of two beads: Bead spacing

Figure 6 illustrates the pressure change along the  $x$  axis and inside air cushions for (a)  $D/r = 1$ ,  $C.A. = 150^\circ$ , (b)  $D/r = 2$ ,  $C.A. = 150^\circ$ , and (c)  $D/r = 2$ ,  $C.A. = 30^\circ$ . In Fig. 6(a), air is trapped between the double beads till the fragmented droplet at the top jump off. As spacing between beads is increased, as shown in Fig. 6(b), intense splashing is captured immediately upon impact, resulting a cluster of small droplets detaching from the original one when the distance between the beads is comparable to the size of the droplet. Eventually, a significant portion of the droplet is trapped between the double beads after the intense splashing. In Fig. 6(c), the droplet splashes and then falls back to the hydrophilic substrate during its expansion, which might capture more air.

It should be noted that air cushions are observed around beads in both Figs. 5 and 6, when the size of the beads is comparable to the size of the droplets. The pressure inside these air cushions falls below atmospheric levels when the covering water is retracting in Fig. 6(a) and rises above the atmospheric levels when the water is spreading in Figs. 5(b) and 6(c).

### V. CONCLUSION

In conclusion, to investigate a droplet impacting on microstructures, a two-dimensional model for numerical simulation is established and validated to analyze the effects of various physical parameters,

including  $We$ ,  $C.A.$ , heights of single hemispherical bead, and distances between double beads on substrates. Distinct force peaks on substrate are captured when either an intact droplet or drop fragments rebound. Droplet rebounding is typically observed at a lower  $We$ , while splashing occurs at a higher  $We$ . When impacting on a single hemispherical bead and if bead size exceeds the droplet size ( $h > r$ ), droplet quickly fragments and splashes, causing force fluctuations. When impacting on double hemispherical beads and if  $D/r = 2$ , a notable amount of water is trapped between the double beads. Furthermore, air cushions are observed around beads when the bead size is comparable to the droplet size, and pressure inside these air cushions fluctuates depending on whether the covering water is retracting or spreading. This comprehensive analysis might provide valuable insights into the complex dynamics and jump-off forces of droplet impacting on various microstructured surfaces, advancing our understanding of the relevant fluid dynamics and offering potential applications in various fields such as erosion protection. In future study, machine learning algorithms can be utilized to develop predictive models for droplet impacting dynamics, which could significantly reduce the computational load and time for complex simulations.

### ACKNOWLEDGMENTS

X.G. acknowledges the funding by the Shanghai Sailing Program from the Science and Technology Commission of Shanghai Municipality (No. 22YF1402500). D.D. acknowledges the funding by the National Program in China and the Startup in Fudan University.

### AUTHOR DECLARATIONS

#### Conflict of Interest

The authors have no conflicts to disclose.

### Author Contributions

**Xi Gu:** Conceptualization (equal); Data curation (lead); Formal analysis (lead); Funding acquisition (lead); Investigation (lead); Methodology (lead); Project administration (lead); Resources (lead); Software (lead); Validation (lead); Visualization (equal); Writing – original draft (lead); Writing – review & editing (equal). **Li Chen:** Investigation (supporting); Validation (supporting); Writing – review & editing (supporting). **Feng Wang:** Conceptualization (supporting); Formal analysis (supporting); Investigation (supporting); Visualization (equal); Writing – review & editing (equal). **Yingrui Wang:** Formal analysis (supporting); Validation (equal). **Yuqi Li:** Data curation (supporting); Investigation (equal); Writing – review & editing (supporting). **Wenna Wu:** Formal analysis (supporting); Writing – review & editing (supporting). **Man Hu:** Conceptualization (equal); Data curation (equal); Formal analysis (equal); Funding acquisition (equal); Writing – review & editing (equal). **Daosheng Deng:** Conceptualization (lead); Funding acquisition (lead); Investigation (equal); Project administration (lead); Supervision (lead); Writing – review & editing (lead).

### DATA AVAILABILITY

The data that support the findings of this study are available from the corresponding authors upon reasonable request.

### REFERENCES

- <sup>1</sup>M. A. Samaha and M. Gad-el Hak, “Slippery surfaces: A decade of progress,” *Phys. Fluids* **33**, 071301 (2021).
- <sup>2</sup>H. Wang, H. Lu, and W. Zhao, “A review of droplet bouncing behaviors on superhydrophobic surfaces: Theory, methods, and applications,” *Phys. Fluids* **35**, 021301 (2023).
- <sup>3</sup>K. Liu and L. Jiang, “Bio-inspired self-cleaning surfaces,” *Annu. Rev. Mater. Res.* **42**, 231–263 (2012).
- <sup>4</sup>J. Lv, Y. Song, L. Jiang, and J. Wang, “Bio-inspired strategies for anti-icing,” *ACS Nano* **8**, 3152–3169 (2014).
- <sup>5</sup>T. M. Schutzius, G. Graeber, M. Elsharkawy, J. Oreluk, and C. M. Megaridis, “Morphing and vectoring impacting droplets by means of wettability-engineered surfaces,” *Sci. Rep.* **4**, 7029 (2014).
- <sup>6</sup>D. Richard and D. Quéré, “Bouncing water drops,” *Europhys. Lett.* **50**, 769 (2000).
- <sup>7</sup>D. Richard, C. Clanet, and D. Quéré, “Contact time of a bouncing drop,” *Nature* **417**, 811–811 (2002).
- <sup>8</sup>J. C. Bird, R. Dhiman, H.-M. Kwon, and K. K. Varanasi, “Reducing the contact time of a bouncing drop,” *Nature* **503**, 385–388 (2013).
- <sup>9</sup>C. Josserand and S. T. Thoroddsen, “Drop impact on a solid surface,” *Annu. Rev. Fluid Mech.* **48**, 365–391 (2016).
- <sup>10</sup>X. Cheng, T.-P. Sun, and L. Gordillo, “Drop impact dynamics: Impact force and stress distributions,” *Annu. Rev. Fluid Mech.* **54**, 57–81 (2022).
- <sup>11</sup>M. A. Nearing, J. M. Bradford, and R. D. Holtz, “Measurement of force vs. time relations for waterdrop impact,” *Soil Sci. Soc. Am. J.* **50**, 1532–1536 (1986).
- <sup>12</sup>B. Zhang, J. Li, P. Guo, and Q. Lv, “Experimental studies on the effect of Reynolds and Weber numbers on the impact forces of low-speed droplets colliding with a solid surface,” *Exp. Fluids* **58**, 125 (2017).
- <sup>13</sup>Q. Lv, J. Li, P. Guo, B. Zhang, and P. Tang, “Effect of Reynolds number on impact force and collision process of a low-velocity droplet colliding with a wall carrying an equal-mass deposited droplet,” *Int. J. Multiphase Flow* **163**, 104432 (2023).
- <sup>14</sup>N. D. Patil, R. Bhardwaj, and A. Sharma, “Droplet impact dynamics on micropillared hydrophobic surfaces,” *Exp. Therm. Fluid Sci.* **74**, 195–206 (2016).
- <sup>15</sup>H. Zhang, X. Zhang, X. Yi, F. He, F. Niu, and P. Hao, “Effect of wettability on droplet impact: Spreading and splashing,” *Exp. Therm. Fluid Sci.* **124**, 110369 (2021).
- <sup>16</sup>H. N. Dalgamoni and X. Yong, “Numerical and theoretical modeling of droplet impact on spherical surfaces,” *Phys. Fluids* **33**, 052112 (2021).
- <sup>17</sup>Y. Wang, Y. Wang, and S. Wang, “Droplet impact on cylindrical surfaces: Effects of surface wettability, initial impact velocity, and cylinder size,” *J. Colloid Interface Sci.* **578**, 207–217 (2020).
- <sup>18</sup>D. Khojasteh, A. Bordbar, R. Kamali, and M. Marengo, “Curvature effect on droplet impacting onto hydrophobic and superhydrophobic spheres,” *Int. J. Comput. Fluid Dyn.* **31**, 310–323 (2017).
- <sup>19</sup>Z. Hu, F. Chu, and X. Wu, “Double-peak characteristic of droplet impact force on superhydrophobic surfaces,” *Extreme Mech. Lett.* **52**, 101665 (2022).
- <sup>20</sup>B. Zhang, V. Sanjay, S. Shi, Y. Zhao, C. Lv, X.-Q. Feng, and D. Lohse, “Impact forces of water drops falling on superhydrophobic surfaces,” *Phys. Rev. Lett.* **129**, 104501 (2022).
- <sup>21</sup>B. Zhang, H. Zhao, Y. Zhao, P. Hao, and C. Lv, “Impact force of ring bouncing on superhydrophobic surface with a bead,” *Phys. Fluids* **35**, 052104 (2023).
- <sup>22</sup>D. Quéré, “Wetting and roughness,” *Annu. Rev. Mater. Res.* **38**, 71–99 (2008).
- <sup>23</sup>C. Antonini, A. Amirfazli, and M. Marengo, “Drop impact and wettability: From hydrophilic to superhydrophobic surfaces,” *Phys. Fluids* **24**, 102104 (2012).
- <sup>24</sup>K. Xu and J. R. Heath, “Contact with what?,” *Nat. Mater.* **12**, 872–873 (2013).
- <sup>25</sup>B. Zhang, C. Ma, H. Zhao, Y. Zhao, P. Hao, X.-Q. Feng, and C. Lv, “Effect of wettability on the impact force of water drops falling on flat solid surfaces,” *Phys. Fluids* **35**, 112111 (2023).
- <sup>26</sup>J. Li, A. Oron, and Y. Jiang, “Droplet jump-off force on a superhydrophobic surface,” *Phys. Rev. Fluids* **8**, 113601 (2023).
- <sup>27</sup>A. Gauthier, S. Symon, C. Clanet, and D. Quéré, “Water impacting on superhydrophobic macrotextures,” *Nat. Commun.* **6**, 8001 (2015).
- <sup>28</sup>M. Abolghasemibizaki, R. L. McMasters, and R. Mohammadi, “Towards the shortest possible contact time: Droplet impact on cylindrical superhydrophobic surfaces structured with macro-scale features,” *J. Colloid Interface Sci.* **521**, 17–23 (2018).
- <sup>29</sup>S. Ding, Z. Hu, L. Dai, X. Zhang, and X. Wu, “Droplet impact dynamics on single-pillar superhydrophobic surfaces,” *Phys. Fluids* **33**, 102108 (2021).
- <sup>30</sup>J. Han, W. Kim, C. Bae, D. Lee, S. Shin, Y. Nam, and C. Lee, “Contact time on curved superhydrophobic surfaces,” *Phys. Rev. E* **101**, 043108 (2020).
- <sup>31</sup>S. Yada, U. Laciş, W. van der Wijngaart, F. Lundell, G. Amberg, and S. Bagheri, “Droplet impact on asymmetric hydrophobic microstructures,” *Langmuir* **38**, 7956–7964 (2022).
- <sup>32</sup>L. Qian, C. Huang, L. Lv, Q. Fu, and C. Fu, “Dynamic behavior of droplets impacting cylindrical superhydrophobic surfaces with different structures,” *Phys. Fluids* **35**, 023331 (2023).
- <sup>33</sup>F. Ai, D. Li, Y. Shang, J. Wang, and L. Shen, “Dynamic simulation of droplet impacting on superhydrophobic surface with cubic protrusion,” *Phys. Fluids* **34**, 092110 (2022).
- <sup>34</sup>S. Bakshi, I. V. Roisman, and C. Tropea, “Investigations on the impact of a drop onto a small spherical target,” *Phys. Fluids* **19**, 032102 (2007).
- <sup>35</sup>P. G. Bange and R. Bhardwaj, “Computational study of bouncing and non-bouncing droplets impacting on superhydrophobic surfaces,” *Theor. Comput. Fluid Dyn.* **30**, 211–235 (2016).
- <sup>36</sup>S. Shen, F. Bi, and Y. Guo, “Simulation of droplets impact on curved surfaces with lattice Boltzmann method,” *Int. J. Heat Mass Transfer* **55**, 6938–6943 (2012).
- <sup>37</sup>D. Zhang, K. Papadakis, and S. Gu, “Investigations on the droplet impact onto a spherical surface with a high density ratio multi-relaxation time lattice-Boltzmann model,” *Commun. Comput. Phys.* **16**, 892–912 (2014).
- <sup>38</sup>X. Liu, Y. Zhao, S. Chen, S. Shen, and X. Zhao, “Numerical research on the dynamic characteristics of a droplet impacting a hydrophobic tube,” *Phys. Fluids* **29**, 062105 (2017).
- <sup>39</sup>H. Liu, S. Krishnan, S. Marella, and H. S. Udaykumar, “Sharp interface Cartesian grid method II: A technique for simulating droplet interactions with surfaces of arbitrary shape,” *J. Comput. Phys.* **210**(1), 32–54 (2005).
- <sup>40</sup>A. A. Abubakar, B. S. Yilbas, G. Hassan, H. Al-Qahtani, H. Ali, and A. Al-Sharafi, “Droplet impacting on a hydrophobic surface: Influence of surface wetting state on droplet behavior,” *J. Fluids Eng.* **142**(7), 071205 (2020).



<sup>41</sup>M. Pasandideh-Fard, G. Tryggvason, and O. A. Basaran, “Capillary effects during droplet impact on a solid surface,” *Phys. Fluids* **8**, 650–659 (1996).

<sup>42</sup>J. Blake, D. Thompson, D. Raps, and T. Strobl, “Simulating the freezing of supercooled water droplets impacting a cooled substrate,” *AIAA J.* **53**(7), 1725–1739 (2015).

<sup>43</sup>H. G. Weller, G. Tabor, H. Jasak, and C. Fureby, “A tensorial approach to computational continuum mechanics using object-oriented techniques,” *Comput. Phys.* **12**, 620–631 (1998).

<sup>44</sup>P. E. Wagner, “Aerosol growth by condensation,” in *Aerosol Microphysics II: Chemical Physics of Microparticles* (Springer, 1982), pp. 129–178.